THE JOURNAL OF PHYSICAL CHEMISTRY C

Article

pubs.acs.org/JPCC

# Charge-Transfer Mechanism in Graphene-Enhanced Raman Scattering

Xi Ling,[†] L. G. Moura,[‡,§] Marcos A. Pimenta,[‡] and Jin Zhang[†,*]

[†]Center for Nanochemistry, Beijing National Laboratory for Molecular Sciences, Key Laboratory for the Physics and Chemistry of Nanodevices, State Key Laboratory for Structural Chemistry of Unstable and Stable Species, College of Chemistry and Molecular Engineering, Peking University, Beijing 100871, China

[‡]Departamento de Fisica, Universidade Federal de Minas Gerais, Belo Horizonte, MG, Brazil 30123970

[§]Departamento de Física, Universidade Federal de Viçosa, Viçosa, MG, Brazil 36570000

Supporting Information

**ABSTRACT:** In the chemical enhancement mechanism for Raman scattering, the two types of charge-transfer models, the excited-state and the ground-state charge-transfer mechanisms, present the different dependence of the enhanced Raman signals on the excitation wavelength. To investigate the type of charge-transfer mechanism in graphene-enhanced Raman scattering (GERS), the Raman excitation profiles of the copper phthalocyanine (CuPc) molecule were obtained in the range of 545—660 nm. The profiles in the GERS system were fitted well with the function of the ordinary resonant Raman scattering expression, where the incident and scattered resonance peaks were well-distinguished with the energy difference equaling the energy of the molecular vibrations. This result meets the prediction of ground-state charge transfer, in which model the dependence of the enhanced Raman signals on the excitation wavelength is the same as that of the ordinary Raman scattering, and rules out the prediction of the excited-state charge transfer because of no the possible charge-transfer resonance peak observed. Therefore, the GERS was proved to be a ground-state charge-transfer mechanism. Meanwhile, because the Raman excitation profiles of molecule can be obtained in the GERS system easily, which is usually difficult to obtain due to the self-absorption of the molecules, GERS opens up a new way to suppress this effect. This work contributes the deeper understanding of the graphene-enhanced Raman scattering.

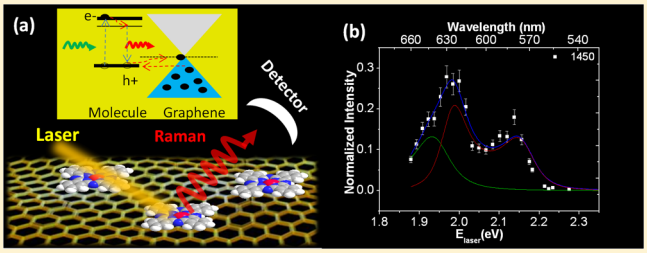


## 1. INTRODUCTION

Since the discovery of graphene-enhanced Raman scattering (GERS) in 2010,[1] GERS has attracted much attention of the scientists. It has been reported that not only pristine graphene,[1−3] but also graphene oxide[4,5] and hydrogen-terminated graphene[6] can perform well in GERS. The enhancement mechanism of GERS as well as the application of graphene in the surface-enhanced Raman scattering (SERS)[7,8] is also a widely discussed issue. In previous work, we have investigated the influence of the different vibrational modes,[1] the distance of graphene and the molecule,[9] the position of the Fermi level of graphene,[10] the interference effect from the $SiO_2$/Si substrate,[11] and the molecular orientation[12] on the intensity of GERS. We attributed the mechanism of GERS to a chemical effect without the disturbance of the electromagnetic mechanism (EM). Recently, Brus et al. have presented a new understanding of the nature of GERS.[13] Moreover, by covering the metal nanoparticle with graphene or graphene derivatives,[6,14−18] it was reported that some problems in traditional metal-based SERS substrate could be overcome, and better Raman-enhanced signals of the adsorbate were obtained, which drove the traditional SERS much closer to the practical application. Now, a deeper understanding of the issues in GERS will be helpful for the development of SERS.

About the chemical enhancement mechanism, at the beginning of the 1980s, Adrian[19] and Lippitsch[20] presented two distinct charge-transfer models, the excited-state charge-transfer model and the ground-state charge-transfer model, respectively. One of the important differences between them is the excitation laser wavelength dependence. For the former, it is usually attributed to the formation of the charge-transfer complex by chemically bonding. The maximum enhancement is usually associated with the transition energy to the charge-transfer resonance state, which depends on the electronic structure of both the molecule and the substrate. For the latter, the charge-transfer complex is not necessary for the Raman enhancement. Charge transfer occurs when the substrate and the molecule are in the ground state because it does not need the help of the light radiation. The maximum enhancement wavelength is dependent on the electronic structure of the molecule itself. Therefore, by measuring the Raman spectra

**Received:** September 5, 2012
**Revised:** October 31, 2012
**Published:** November 2, 2012






dx.doi.org/10.1021/jp3088447 | J. Phys. Chem. C 2012, 116, 25112−25118

under the serials of laser wavelengths and then obtaining the Raman excitation profile, the type of charge-transfer mechanism can be attributed. The technique, used for studying the mechanism of SERS by the Raman excitation profile, is called the wavelength-scanned Raman excitation spectroscopy. Van Duyne and Moskovits have investigated the EM in SERS using the technique successfully, and it was established as a useful tool.[21−24]

Herein wavelength-scanned Raman measurement of copper phthalocyanine (CuPc) molecule was carried out in both the non-GERS (here the non-GERS system refers to the pristine Langmuir−Blodgett (LB) film of the CuPc molecules on a $SiO_2$/Si substrate or the CuPc powder) and GERS systems. The phthalocyanine derivative is an important optical function material[25] and has been used in a wide field, such as the organic field effect transistor,[26−28] nonlinear optics,[29] and so on. Most of the superior properties of phthalocyanine derivative are dominated by the so-called Q-band, which is a characteristic absorption band of phthalocyanine derivative, which originates from the $\pi-\pi^*$ transition.[25,30−32] It appears in the visible range and usually splits into two peaks because of the Jahn−Teller effect.[30] As the viewpoint of the excited-state charge transfer,[19] for the CuPc/graphene system, if the excited-state charge-transfer mechanism dominates, then there should be a charge-transfer resonance peak at ∼1.9 eV (considering that the Fermi level of graphene is at −4.6 eV and the HOMO and LUMO of CuPc are at −4.9 and −2.7 eV; here we ignored the small change of the energy band of graphene and the molecule because the UV−visble spectra showed less difference between the GERS and non-GERS system),[32,33] whereas if the ground-state charge-transfer mechanism dominates, then the Raman excitation profile should follow the ordinary Raman resonant profile of the molecule. Therefore, we performed Raman measurement by changing the laser excitation wavelength in the range of 545—660 nm (2.27 to 1.88 eV), which corresponds to the Q-band absorption region. By analyzing the obtained Raman excitation profiles, the type of charge-transfer mechanism in GERS can be determined.

## 2. EXPERIMENTAL DETAILS

**2.1. Graphene Preparation.** Graphene was prepared by the mechanical exfoliation of Kish graphite (Covalent Materials Corp.) using scotch tape on a $SiO_2$/Si substrate (300 nm thick oxide). Monolayer graphene was characterized by optical microscopy (OM) and Raman spectroscopy as we did before.[1]

**2.2. Non-GERS and GERS Samples.** CuPc powder purchased from Alfa Aesar was used directly. Both the CuPc LB film deposited on a 300 nm $SiO_2$/Si substrate and the CuPc powder were used as a reference for the GERS investigation and are named the non-GERS samples. The LB film of CuPc was prepared as our previous work.[9,12] In the GERS sample, 2 Å of CuPc molecules was deposited on the graphene on the top of a 300 nm $SiO_2$/Si substrate by the vacuum thermal deposition (CuPc/graphene/$SiO_2$/Si). Therefore, most of the molecules are isolated from each other in the environment.

**2.3. Raman Measurement.** Wavelength-scanned Raman measurements were carried out in the non-GERS and GERS samples using a Dilor XY triple spectrometer. The Raman excitation profiles of the CuPc molecule were obtained by figuring the Raman intensity as a function of the excitation laser energy. The Raman intensity of all peaks from the CuPc molecule are normalized by the Raman signal at 802 $cm^{-1}$ from cyclohexane, which was collected under the same experimental conditions. The intensities of the peaks are obtained by fitting with a Lorentzian function. Both the Raman signals from CuPc molecule and the liquid cyclohexane (cyclohexane was filled in a quartz cuvette) were collected using the backscattering geometry, and an Olympus microscope was used to focus the incident light on the sample, with a spot size of ∼1 $\mu m^2$. The dye laser pumped by 6 W from Ar+ laser was used to obtain the continuous tunable laser lines from 545 to 660 nm, depending on the dye. Here three types of dyes were used to obtain the different laser lines: (1) DCM (4-(dicyanomethylene)-2-methyl-6-(*p*-dimethylamino-styryl)-4*H*-pyran) dye from 610 to 660 nm; (2) R6G (Rhodamine dye) from 570 to 620 nm; and (3) R6G dye from 545 to 560 nm. Raman measurements were carried out using steps of 5 nm for the laser excitations in the range 545−660 nm. The laser power was controlled at 1.0 ± 0.1 mW to avoid the heating effect and the desorption of the molecules. The exposed time was typically 30 s, and 5 accumulations were used to ensure the high signal-to-noise ratio. The Raman spectra were collected in the range of 200−1700 $cm^{-1}$.

## 3. RESULTS AND DISCUSSION

**3.1. Raman Spectra of CuPc Molecule under Different Excitation Wavelengths.** It is well known the Raman scattering process can be illustrated by the Feynman figure, as shown in Figure 1, from which it is explained that the Raman

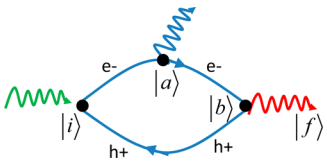


**Figure 1.** Feynman figure of the Raman scattered process.

scattering process experienced the following three steps as the quantum theory: (1) the incident light interacts with the electron in the ground state; (2) the excited electron couples to the phonon (or vibrational mode); and (3) the electron backs to the ground state and radiates the scattered light. Every step can be described using a matrix element of the respective Hamiltonians and contributes positively to Raman scattered intensity. For the ordinary resonant Raman scattering, the Raman scattered intensity (considering the Stokes Raman scattering process) can be expressed as:[34,35]

$$I(E_L) = K\left|\frac{\langle f|H_{e-r}|b\rangle\langle b|H_{e-ph}|a\rangle\langle a|H_{e-r}|i\rangle}{(E_L - E_g - i\Gamma_a)(E_L - E_{ph} - E_g - i\Gamma_b)}\right|^2 \quad (1)$$

where $|i\rangle$ is the initial state, $|a\rangle$ and $|b\rangle$ are two intermediate states, $|f\rangle$ is the final state; $H_{e-r}$ and $H_{e-ph}$ are the matrix element of the respective Hamiltonians of the radiation of the light and the electron−phonon coupling, respectively; $E_L$ is the energy of the incident light; $E_g$ is the energy of the electron transition; $E_{ph}$ is the energy of the phonon (or vibrational mode); and $\Gamma_a$ and $\Gamma_b$ are the damping constants, which are related with the lifetimes of the two intermediate states $|a\rangle$ and $|b\rangle$. From the denominator of the eq 1, the Raman intensity depends on the excitation laser energy $E_L$, and the Raman intensity can get to a maximum when $E_L = E_g$ or $E_L = E_g + E_{ph}$.

Figure 2 shows the Raman spectra of CuPc in the non-GERS and GERS samples, obtained by changing the laser excitation


dx.doi.org/10.1021/jp3088447 | J. Phys. Chem. C 2012, 116, 25112−25118

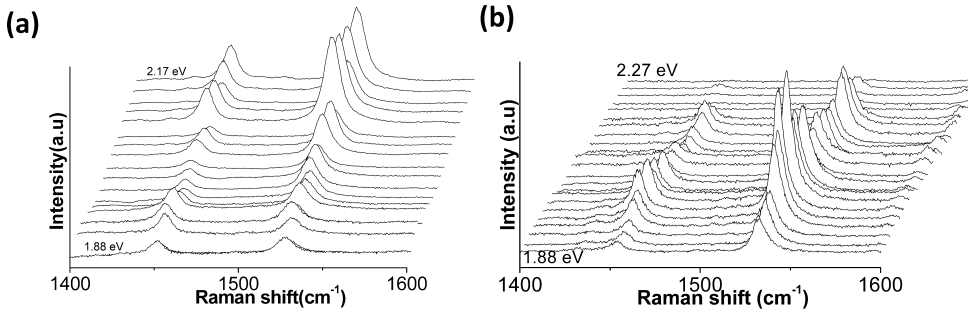


**Figure 2.** Serials of Raman spectra of CuPc molecules in the non-GERS system (a) excited by the laser lines from 660 to 570 nm and in the GERS system (b) excited by the laser lines from 660 to 545 nm. Raman measurement was carried out every 5 nm in the corresponding range. For clear display, only the spectra in the range of 1400−1600 $cm^{-1}$ were shown.

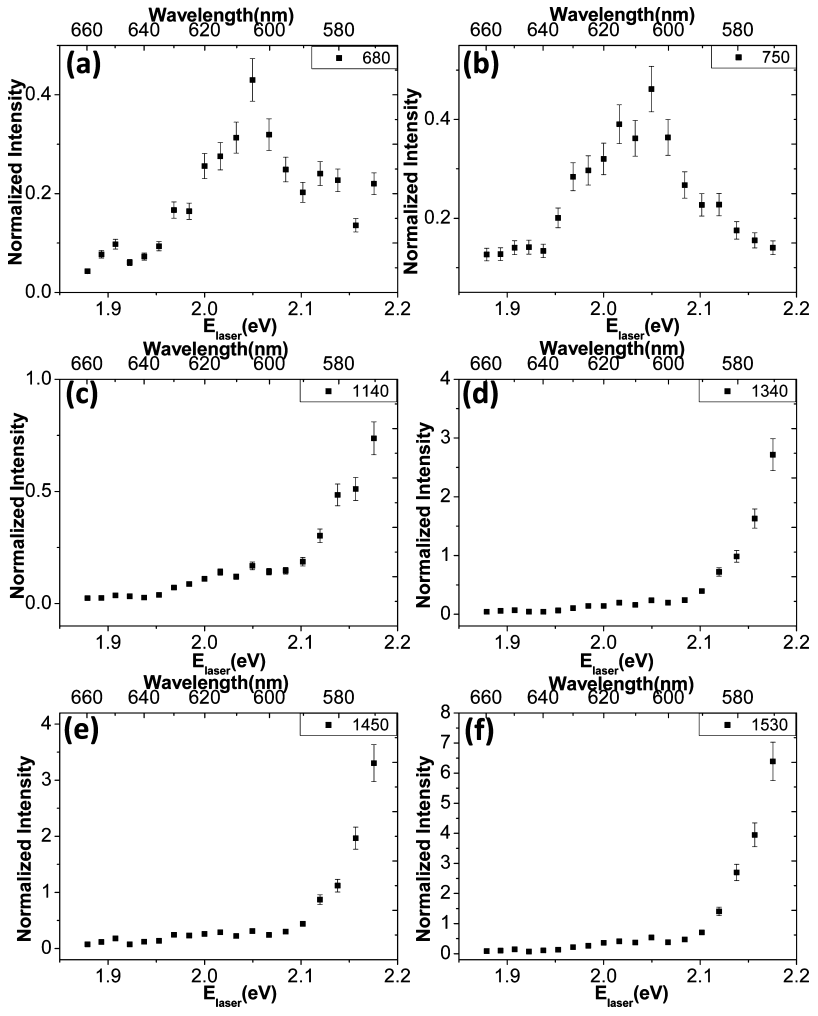


**Figure 3.** Raman excitation profiles of different vibrational modes of CuPc in the non-GERS system. The corresponding peak positions are shown on the upper right corner. The error bar is from the uncertainty of the laser power.

every 5 nm from 660 to 545 nm. (For the non-GERS system, it is from 660 to 570 nm.) For both of them, the Raman intensities of CuPc Raman signals vary with the excitation wavelength. Usually, the variation of the Raman intensity with the excitation wavelength depends on several factors, such as the change of the Raman scattering cross section and the self-absorption of the molecule to the scattered light. In the first case, because the absorption of the molecule is different at different wavelengths, the strength of the first step in the Feynman figure (the incident light interacts with the electron) is different, which induces the different Raman scattering cross sections.[34,35] In the second case, the self-absorption of the molecule to the scattered light decreased the intensity of the Raman signal into the detector.[36] Ordinarily, according to the Fermi's gold rule,[37] the intensity of the Raman scattering is proportional to the probability of the transitions involved in the Raman process, and the transition probability will be large when the excitation energy is equal to the electron transition energy, where it usually corresponds to a absorption peak in the UV−visible absorption spectroscopy. Therefore, if there is no


dx.doi.org/10.1021/jp3088447 | J. Phys. Chem. C 2012, 116, 25112−25118

self-adsorption, then the ordinary Raman excitation profile should be dependent on the absorption profile with an incident resonance peak at the maximum absorption ($E_L = E_g$) in addition to a scattered resonance peak at $E_L = E_g + E_{ph}$. The range of the used wavelength corresponds to the Q-band absorption region of the CuPc molecule, where the absorption peaks appear at about 626 (1.98 eV) and 700 nm (1.77 eV). (See part 1 in the Supporting Information.) Therefore, in this work, the CuPc molecules should have an incident resonance peak at ~1.98 eV and a scattered resonance peak at higher energy depending on the energy of the vibrational mode.

**3.2. Raman Excitation Profiles of CuPc Molecule in the non-GERS System.** Figure 3 shows the Raman excitation profiles of different vibrational modes of CuPc in the non-GERS system (CuPc LB film/$SiO_2$/Si). Here six vibrational modes, 680, 750, 1140, 1340, 1450, and 1530 $cm^{-1}$, which can be assigned accurately,[25,31,36] are analyzed. The assignment and the corresponding energy of the vibrational modes are shown in Table 1. The vibrational modes at 650 and 750 $cm^{-1}$ are both

**Table 1. Assignment and the Corresponding Energy of the Vibrations in CuPc Molecule**

| peak ($cm^{-1}$) | $E_{vibration}$ (eV) | symmetry assignment | mode description |
|---|---|---|---|
| 679.0 | 0.085 | $A_{1g}$ | macrocycle breathe symmetrically |
| 747.2 | 0.092 | $B_{1g}$ | deformation of the macrocycle |
| 1140.4 | 0.142 | $B_{2g}$ | deformation of the isoindole ring system |
| 1341.8 | 0.166 | $A_{1g}$ | symmetric vibration of isoindole ring |
| 1453.8 | 0.18 | $B_{2g}$ | deformation of the isoindole ring system |
| 1530.8 | 0.19 | $A_{1g}$ | symmetric stretching motion of isoindole groups |

attributed to the breathing vibrations of the macrocycle. Notice in Figure 3 the existence of a weak peak at ~2.05 eV and a shoulder peak at ~1.98 eV, which are attributed to the scattered resonance peak and the incident resonance peak, respectively. The other four vibrational modes are attributed to the motions of the isoindole rings. There is no resonance peak in the Q-band region. The data show that it is difficult to get the Raman excitation profile of the Q-band of CuPc molecules in the non-GERS system, especially for the range of the red band (which induces an apparent increase in the profiles in the high-energy region, as shown in Figure 3c–f).[36] Similarly to the case of the CuPc LB film/$SiO_2$/Si system, the CuPc powder shows similar Raman excitation profiles, as shown in the part 2 in the Supporting Information. This is attributed to the self-absorption of CuPc molecules, which was an obstacle in investigating the electronic property of CuPc by Raman spectroscopy in the previous study.[36]

**3.3. Raman Excitation Profiles of CuPc Molecule in the GERS System.** Differently from the non-GERS system, distinguished Raman excitation resonant profile can be obtained in the GERS system, as shown in Figure 4. First, the profiles in the GERS system are completely different from that in the non-GERS system, which is consistent with the fact that the graphene substrate can influence the Raman signals of CuPc molecule.[1,12] In addition, the profiles for different vibrational modes are different from each other. It was found that the profiles can be fitted well by the expression function of the ordinary resonant Raman intensity, as shown in eq 1. When fitting, $I(E_L)$ and $E_L$ are variable, and $A$, $E_g$, $E_{ph}$, $\Gamma_a$, and $\Gamma_b$ are five fitting parameters. $A$ is defined as $(K\langle f|H_{e-r}|b\rangle\langle b|H_{e-ph}|a\rangle\langle a|H_{e-r}|i\rangle)^2$, which is a constant when the system is fixed. By fixing $E_g$ = 1.98 eV or 1.77 eV and $E_{ph}$ equal to the corresponding energy of the vibration, all of the profiles in Figure 4 can be well-fitted with the related coefficients $R^2$ showing on the up right corner. The fitting parameters are shown in the part 3 in the Supporting Information. The red lines correspond to the profiles for the vibrational modes with energy $E_g$ = 1.98 eV, and the green line corresponds to the profile for $E_g$ = 1.77 eV. From the red fitting curve, both the incident resonant profile and the scattered resonant profile can be well-distinguished, with the energy difference equaling the energy of the molecular vibrations. The difference between the GERS system and the non-GERS system, as well as the different vibrational modes, can also be clearly displayed by considering the variation of the relative Raman intensity of the modes as a function of the excitation laser energy. (See the part 4 in the Supporting Information.) For low-frequency vibrational modes, because the vibrational energy is small, the scattered resonance peak is close to the incident resonance peak, which induces the overlap of the two peaks. With the increase in the frequencies of the vibrational modes, the scattered resonance peak is gradually far away from the incident resonance peak, and they can be clearly distinguished in the resonance Raman profile. Besides, because of the limitation of the available laser lines, there is not enough data to cover the range of profile corresponding to $E_g$ = 1.77 eV vibrational modes. Only a part of the scattered resonant profiles can be seen, as shown by the green line, where the peak blue shifts with the increase in the vibration energy. This is consistent with the prediction of the resonant Raman scattering. Furthermore, the GERS sample with the lying-down CuPc molecule on graphene constructed by annealing the CuPc LB/graphene/$SiO_2$/Si was also investigated. It shows a similar Raman excitation profile as Figure 4, as shown in the part 5 in the Supporting Information.

Considering the red profiles, which correspond to vibrational modes with energy $E_g$ = 1.98 eV, the fitting results are listed in Table 2. It can be seen that the maxima of the profiles are not exactly the same as the theoretical values, but with the incident resonance peak blue-shifted and the scattered resonance peak red-shifted. This is because of the interference of the two terms in the denominator of the eq 1. Moreover, for different vibrational modes, the relative intensity of the incident and scattered resonance peaks is much different. As shown Table 2, for the vibrations at 1140 and 1340 $cm^{-1}$, they have the scattered resonance peak stronger than the incident resonance peak, whereas for the vibrations at 1450 and 1530 $cm^{-1}$, they have the opposite relative intensity, with the incident resonance peak stronger than the scattered resonance peak. This effect originates from the different lifetimes of the two intermediate states of the Raman process.

**3.4. Charge-Transfer Mechanism in the GERS System.** As the prediction of the two types of charge-transfer models, the profiles in Figure 4 are fitted well using the function of the ordinary resonant Raman intensity expression; meanwhile, the GERS system and spectra own some other characters consistent with the ground-state charge-transfer model (which was discussed in the following statement); the charge transfer in GERS is attributed to the ground-state charge-transfer. Moreover, we did not observe the possible charge-transfer resonance-peak (at 1.90 eV) in the profiles, and this result is not consistent with the excited-state charge-transfer model.


dx.doi.org/10.1021/jp3088447 | J. Phys. Chem. C 2012, 116, 25112–25118

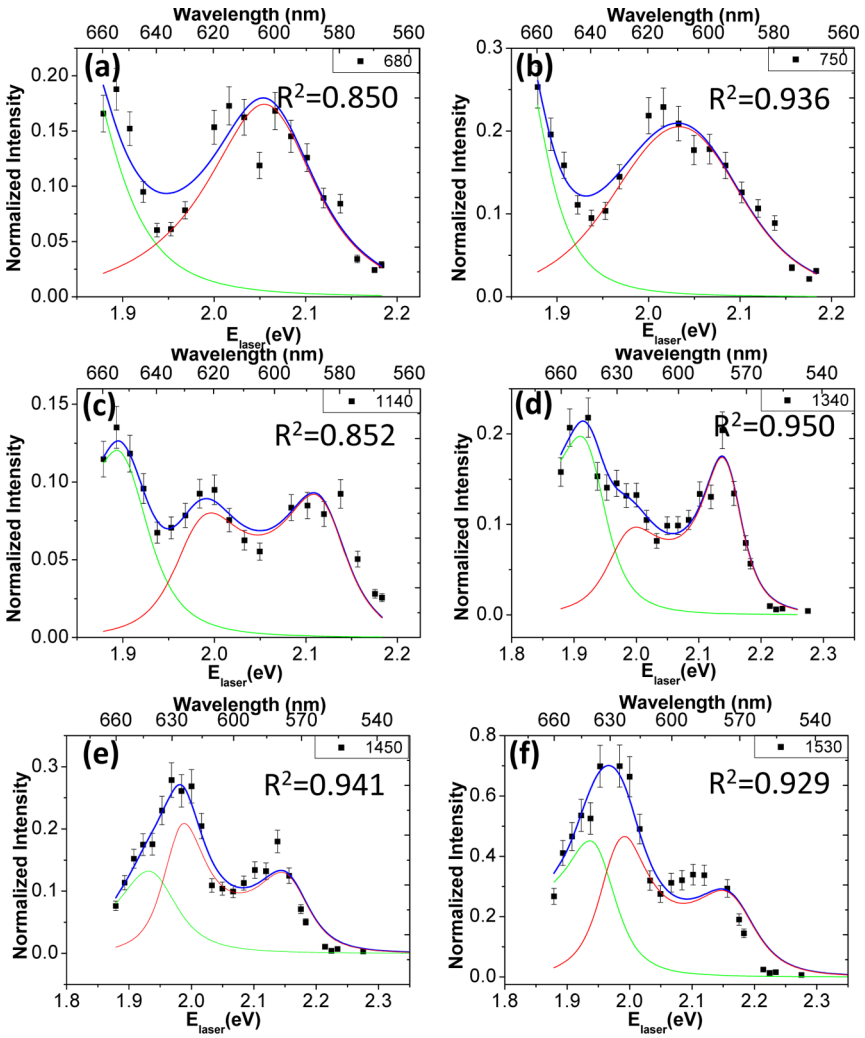


**Figure 4.** Raman excitation profiles of different vibrational modes of CuPc in the GERS system. The red and green lines are the two curves used to fit the data. The blue lines are the results of the fitting. The corresponding peak positions and fitting related coefficients are shown on the upper right corner. The error bar is from the uncertainty of the laser power. For some laser lines excitation, because some Raman vibrational modes are too weak to get, the data are not shown.

**Table 2. Fitting Results of the Raman Excitation Profiles of CuPc Vibrational Modes in the GERS system (Only the Profiles Corresponding to the $E_g$ = 1.98 eV were Considered (the red lines in Figure 4))**

| peak ($cm^{-1}$) | $E_{vibration}$ (eV) | theoretical $E_{scattered}$ (eV) | experimental $E_{incident}$ (eV) | experimental $E_{scattered}$ (eV) | $I_{incident}$ | $I_{scattered}$ | $R^2$ |
|---|---|---|---|---|---|---|---|
| 679.0 | 0.085 | 2.065 | ---[a] | --- | --- | --- | 0.850 |
| 747.2 | 0.092 | 2.072 | --- | --- | --- | --- | 0.936 |
| 1140.4 | 0.142 | 2.122 | 1.99 | 2.11 | 0.08 | 0.09 | 0.852 |
| 1341.8 | 0.166 | 2.145 | 2.00 | 2.13 | 0.10 | 0.17 | 0.950 |
| 1453.8 | 0.180 | 2.160 | 1.99 | 2.15 | 0.21 | 0.13 | 0.941 |
| 1530.8 | 0.190 | 2.170 | 1.99 | 2.15 | 0.47 | 0.29 | 0.929 |

[a]Data are difficult to get because the incident and scattered resonance peaks are overlapped.

Therefore, by using the wavelength-scanned Raman excitation spectroscopy technique, we concluded that the charge-transfer mechanism in the GERS system was dominated by the ground-state charge transfer.

For the three steps of the Feynman process, every step enhanced can induce the enhancement of the Raman signals. In the CuPc/Graphene system, the Fermi level of graphene (−4.6 eV) is close to the HOMO of CuPc (−4.9 eV).[32,33] Meanwhile, the aza-nitrogen lone-pair electrons orbitals were reported to lie at around −4.9 eV, near the HOMO of CuPc.[38] Ground-state charge transfer can easily happen between them because the $\pi$ electrons are abundant on the surface of graphene and the energy band of graphene is continuous. Therefore, the ground-state charge-transfer process in the GERS system can be speculated, as shown in Figure 5. The electrons in graphene can be involved in the Raman-scattered process of CuPc molecules and enhance the process of electron−phonon coupling (step 2 in the Feynman figure), which induces the enhancement of the Raman signals as eq 1.


dx.doi.org/10.1021/jp3088447 | J. Phys. Chem. C 2012, 116, 25112−25118

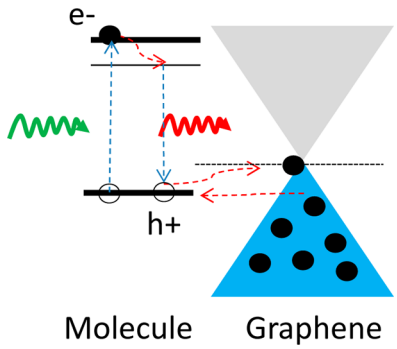


**Figure 5.** Schematic analysis of the Raman scattered process of GERS.

It should be noted that most of works on chemical mechanism are discussed using the excited-state charge-transfer model because they are usually in a traditional SERS system based on the metal substrate and the molecules are usually chemically bonded on the surface of the metal, where the electronic structure of the system is strongly changed.[39−43] The resonance condition changed after the molecule is bonded on the surface of the metal, and the incident light could drive the charge-transfer transition between the metal and the molecule, inducing the enhancement of the Raman signal. The strongest vibrational mode enhancement is usually related to the vibration involving atoms that are close to the metal−molecule bond. Here, in the GERS system, it is physical interaction that occurs between graphene and the molecules, and there is no chemical bonding between them. The electronic structure of the molecule will not change too much (as described from the UV−visible absorption spectra in our recent work[12]). The strongest vibrational mode enhancement occurs for the vibrational mode involving the lone pair or $\pi$ electrons, which has stronger coupling with graphene.[12]

**3.5. Suppression of the Self-Absorption Effect of CuPc in the GERS System.** In addition, it is necessary to emphasize that, compared with the non-GESR system, the GERS system is helpful to obtain the detailed Raman excitation profiles in the Q-band region. Requiring the detailed Q-band structure by the Raman resonant profile is valuable because Raman spectroscopy can provide more detailed information than other characterization tools, such as the UV−visible absorption spectroscopy.[36] However, the self-absorption of the incident and scattered radiation limited the obtaining of the Raman resonant profile in the CuPc powder (or other dye molecules).[36,44] As shown in Figure 6a, because the CuPc molecules $\pi-\pi$ interacted with each other in the powder, there is multimode coupling between them. This induces the self-absorption in which the scattered light from one CuPc molecule is absorbed by the nearby CuPc molecule, weakening the signal of the scattered light into the detector. In previous work, as reported by Bovill et al.,[36,44] the way used to overcome the problem was carrying out the measurement at the electrode or metal surface or at the low temperature, which can supply a constrained environment to the CuPc molecule and suppress the multimode interaction-induced self-adsorption. Here, in the GERS system, by placing the CuPc molecule on graphene, obviously, we can obtain the Raman excitation profiles of CuPc molecule easily. It is contributed to the two key roles of graphene in the GERS system, as shown in Figure 6b: (1) graphene supplies a constrained environment to the CuPc molecule through the $\pi-\pi$ interaction, which can lower the vibrational amplitudes and reduce the possibility of sufficient freedom for multimode interaction and suppress the self-absorption of the CuPc molecules; (2) graphene enhances the Raman signals of the contacted molecule by chemical mechanism, which is convenient to obtain the Raman signals from very few numbers of the molecules. Both of them induce the enhancement of the Raman signals and the acquisition of the Raman excitation profiles of CuPc. Meanwhile, compared with the profiles obtained by Bovill et al.[36] at the low temperature (10 K), where only the incident resonance peak was obtained, the measurement using the GERS method was carried out under a much softer condition, and both the incident and scattered resonance peaks were obtained. It indicates that GERS is a better technique to obtain the Raman excitation profiles of the molecule.

## 4. CONCLUSIONS

In conclusion, with the assistance of the wavelength-scanned Raman excitation spectroscopy technique, by analyzing the Raman excitation profiles of the CuPc molecule, we attributed the type of charge-transfer mechanism in the GERS system to a ground-state charge transfer. The profiles can be fitted well with the function of the ordinary resonant Raman scattering expression, where the incident and scattered resonance peaks were well-distinguished with the energy difference equaling the energy of the molecular vibrations. In addition, it opened up a new way to obtain the Raman excitation profile of the molecule by using the GERS technique because the constrained environment supplied by graphene can suppress the self-absorption of the molecule, and this effect is helpful to the acquisition of the Raman excitation profiles.

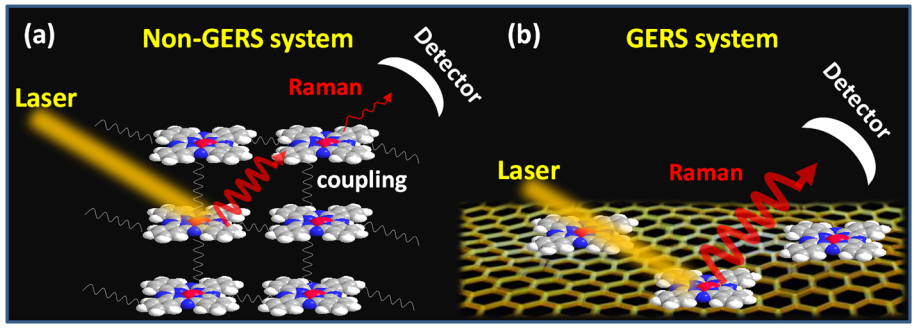


**Figure 6.** Schematic illustration of the situation of the self-adsorption in the non-GERS (a) and GERS (b) systems.


dx.doi.org/10.1021/jp3088447 | J. Phys. Chem. C 2012, 116, 25112−25118

## ■ ASSOCIATED CONTENT

### Supporting Information

UV−visible absorption spectroscopy of CuPc, Raman profiles of the CuPc powder, the fitting parameters of the profiles in the GERS system, the variation of the relative Raman intensity of the modes of CuPc molecule as the excitation laser energy, and Raman excitation resonant profiles of lying-down CuPc on graphene constructing by annealing the CuPc LB/graphene/$SiO_2$/Si. This material is available free of charge via the Internet at http://pubs.acs.org.

## ■ AUTHOR INFORMATION


### Corresponding Author

*Tel/Fax: 86-10-6275-7157. E-mail: jinzhang@pku.edu.cn.


### Notes

The authors declare no competing financial interest.

## ■ ACKNOWLEDGMENTS

This work was supported by MOST (2011YQ0301240201 and 2011CB932601), NSFC (50972001, 21233001 and 51121091), and the Brazilian agencies Fapemig and CNPq (INCT Nanomateriais de Carbono).

## ■ REFERENCES


(1) Ling, X.; Xie, L. M.; Fang, Y.; Xu, H.; Zhang, H. L.; Kong, J.; Dresselhaus, M. S.; Zhang, J.; Liu, Z. F. *Nano Lett.* **2010**, *10* (2), 553−561.

(2) Qiu, C. Y.; Zhou, H. Q.; Yang, H. C.; Chen, M. J.; Guo, Y. J.; Sun, L. F. *J. Phys. Chem. C* **2011**, *115* (20), 10019−10025.

(3) Peimyoo, N.; Yu, T.; Shang, J. Z.; Cong, C. X.; Yang, H. P. *Carbon* **2012**, *50*, 201−208.

(4) Huh, S.; Park, J.; Kim, Y. S.; Kim, K. S.; Hong, B. H.; Nam, J. M. *ACS Nano* **2011**, *5* (12), 9799−9806.

(5) Yu, X. X.; Cai, H. B.; Zhang, W. H.; Li, X. J.; Pan, N.; Luo, Y.; Wang, X. P.; Hou, J. G. *ACS Nano* **2011**, *5* (2), 952−958.

(6) Liu, C. Y.; Liang, K. C.; Chen, W. L.; Tu, C. H.; Liu, C. P.; Tzeng, Y. *Opt. Express* **2011**, *19* (18), 17092−17098.

(7) Campion, A.; Kambhampati, P. *Chem. Soc. Rev.* **1998**, *27* (4), 241−250.

(8) Kneipp, K.; Kneipp, H.; Moskovits, M. *Surface-Enhanced Raman Scattering: Physics and Applications*; Springer-Verlag: Berlin, 2006.

(9) Ling, X.; Zhang, J. *Small* **2010**, *6* (18), 2020−2025.

(10) Xu, H.; Xie, L. M.; Zhang, H. L.; Zhang, J. *ACS Nano* **2011**, *5* (7), 5338−5344.

(11) Ling, X.; Zhang, J. *J. Phys. Chem. C* **2011**, *115* (6), 2835−2840.

(12) Ling, X.; Wu, J. X.; Xu, W. G.; Zhang, J. *Small* **2012**, *8* (9), 1365−1372.

(13) Thrall, E. S.; Crowther, A. C.; Yu, Z. H.; Brus, L. E. *Nano Lett.* **2012**, *12* (3), 1571−1577.

(14) Zhao, H.; Fu, H. G.; Zhao, T. S.; Wang, L.; Tan, T. X. *J. Colloid Interface Sci.* **2012**, *375*, 30−34.

(15) Hao, Q. Z.; Wang, B.; Bossard, J. A.; Kiraly, B.; Zeng, Y.; Chiang, I. K.; Jensen, L.; Werner, D. H.; Huang, T. J. *J. Phys. Chem. C* **2012**, *116* (13), 7249−7254.

(16) Chen, P.; Yin, Z. Y.; Huang, X.; Wu, S. X.; Liedberg, B.; Zhang, H. *J. Phys. Chem. C* **2011**, *115* (49), 24080−24084.

(17) Liu, X. J.; Cao, L. Y.; Song, W.; Ai, K. L.; Lu, L. H. *ACS Appl. Mater. Inter.* **2011**, *3* (8), 2944−2952.

(18) Xu, W. G.; Ling, X.; Xiao, J. Q.; Dresselhaus, M. S.; Kong, J.; Xu, H. X.; Liu, Z. F.; Zhang, J. *Proc. Natl. Acad. Sci. U.S.A.* **2012**, *109* (24), 9281−9286.

(19) Adrian, F. J. *J. Chem. Phys.* **1982**, *77* (11), 5302−5314.

(20) Lippitsch, M. E. *Phys. Rev. B* **1984**, *29* (6), 3101−3110.

(21) Zhao, J.; Dieringer, J. A.; Zhang, X. Y.; Schatz, G. C.; Van Duyne, R. P. *J. Phys. Chem. C* **2008**, *112* (49), 19302−19310.

(22) Vlckova, B.; Gu, X. J.; Moskovits, M. *J. Phys. Chem. B* **1997**, *101* (9), 1588−1593.

(23) Ye, J.; Hutchison, J. A.; Uji-i, H.; Hofkens, J.; Lagae, L.; Maes, G.; Borghs, G.; Van Dorpe, P. *Nanoscale* **2012**, *4* (5), 1606−1611.

(24) McFarland, A. D.; Young, M. A.; Dieringer, J. A.; Van Duyne, R. P. *J. Phys. Chem. B* **2005**, *109* (22), 11279−11285.

(25) Tackley, D. R.; Dent, G.; Smith, W. E. *Phys. Chem. Chem. Phys.* **2001**, *3* (8), 1419−1426.

(26) Cao, Y.; Wei, Z. M.; Liu, S.; Gan, L.; Guo, X. F.; Xu, W.; Steigerwald, M. L.; Liu, Z. F.; Zhu, D. B. *Angew. Chem., Int. Ed.* **2010**, *49* (36), 6319−6323.

(27) Blumenfeld, M. L.; Steele, M. P.; Monti, O. L. A. *J. Phys. Chem. Lett.* **2010**, *1* (1), 145−148.

(28) Xiao, K.; Liu, Y. Q.; Huang, X. B.; Xu, Y.; Yu, G.; Zhu, D. B. *J. Phys. Chem. B* **2003**, *107* (35), 9226−9230.

(29) Papageorgiou, N.; Salomon, E.; Angot, T.; Layet, J. M.; Giovanelli, L.; Le Lay, G. *Prog. Surf. Sci.* **2004**, *77* (5−8), 139−170.

(30) Farag, A. A. M. *Opt. Laser Technol.* **2007**, *39* (4), 728−732.

(31) Liu, Z.; Zhang, X.; Zhang, Y.; Jiang, J. *Spectrochim. Acta, Part A* **2007**, *67* (5), 1232−1246.

(32) Liao, M. S.; Scheiner, S. *J. Comput. Chem.* **2002**, *23* (15), 1391−1403.

(33) Aristov, V. Y.; Molodtsova, O. V.; Maslyuk, V.; Vyalikh, D. V.; Zhilin, V. M.; Ossipyan, Y. A.; Bredow, T.; Mertig, I.; Knupfer, M. *Appl. Surf. Sci.* **2007**, *254* (1), 20−25.

(34) Ferraro, J. R.; Nakamoto, K.; Brown, C. W. *Introductory Raman Spectroscopy*; Elsevier: New York, 2003; Vol. *1*.

(35) Yu, P. Y.; Cardona, M. *Fundamentals of Semiconductors: Physics and Materials Properties*; Springer-Verlag: Heidelberg, 2005.

(36) Bovill, A. J.; Mcconnell, A. A.; Nimmo, J. A.; Smith, W. E. *J. Phys. Chem* **1986**, *90* (4), 569−575.

(37) Lu Ru, E. C.; Etchegoin, P. G. *Principles of Surface-Enhanced Raman Spectroscopy and Related Plasmonic Effects*; Elsevier: Oxford, U.K., 2009; Vol. *4*.

(38) Mack, J.; Stillman, M. J. *J. Phys. Chem* **1995**, *99* (20), 7935−7945.

(39) Nakai, H.; Nakatsuji, H. *J. Chem. Phys.* **1995**, *103* (6), 2286−2294.

(40) Otto, A.; Futamata, M. *Top. Appl Phys.* **2006**, *103*, 147−182.

(41) Sun, M. T.; Liu, S. S.; Chen, M. D.; Xu, H. X. *J. Raman Spectrosc.* **2009**, *40* (2), 137−143.

(42) Sun, M. T.; Liu, S. S.; Li, Z. P.; Duan, J. M.; Chen, M. D.; Xu, H. X. *J. Raman Spectrosc.* **2009**, *40* (9), 1172−1177.

(43) Sun, M. T.; Wan, B. S.; Liu, Y. J.; Jia, Y.; Xu, H. X. *J. Raman Spectrosc.* **2008**, *39* (3), 402−408.

(44) Bovill, A. J.; Mcconnell, A. A.; Smith, W. E. *J. Chem. Soc., Faraday Trans.* **1990**, *86* (24), 4065−4069.